Biogeotechnics 4 (2026) 100180

Contents lists available at ScienceDirect

Biogeotechnics

journal homepage: www.keaipublishing.com/en/journals/biogeotechnics/

# Hydrophobic sand erodibility remediation with biopolymers under long-term environmental conditions

Jonathon Chavez De Rosas, Ingrid Tomac*

*University of California San Diego, 9500 Gilman Drive, La Jolla, CA 92093, USA*

ARTICLE INFO

*Keywords:*
Post-wildfire erosion
Erosion mitigation
Xantham gum
Debris flow
Hydrophobic sand improvement

ABSTRACT

This paper investigates the advantages and limitations of hydrophobic sand surficial improvement using bio-treatments. Xantham gum (X.G.) at different concentrations in sand represents the biopolymer class of materials. The study aims to simulate wildfire-burned sands through highly hydrophobic sands at various high and low-rain-intensity slopes in controlled experimental conditions. In addition, a 6-month exposure to environmental conditions like wind, rain, tree debris, and animal interactions assesses the effectiveness of long-term treatment. Results show that sand type is a governing parameter, and fine sands require the highest X.G. percentage. During prolonged rain, surface morphology evolves with ridges that can fail. Results show that, at a 50 mm/h rain, when left uncured, the XG-soil mix provides catastrophic erosion, more so than untreated hydrophobic sand, while those with 1 %–3 % X.G. concentrations in the mixed layer cured for 24 h yielded significantly less erosion. Therefore, the study proposes covering hydrophobic slopes with X.G. and hydrophilic sand mix sprayed with 16.5 % water per X.G. and sand mix mass and cured for 24 h. During environmental studies, initial treatments of uncured 0.5 % X.G. mixed with sand provided little erosion reduction compared to the unmitigated hydrophobic slopes but mostly observed even more erosion. With fully formed channels in the slopes, the top layer, re-covered with a 3 % XG-sand mix and cured, shows the effects of the mitigation technique on previously eroded slopes. At a higher intensity than the previous storms, this method performs better than the 0.5 % X.G. uncured mix, but overwetted sections that were not dry before the next storm led to enhanced erosion. Cumulative erosion between rain events reveals similar erosion trends between the three sand types, with fine sand slopes eroding slightly more.

## 1. Introduction

This paper presents a comprehensive experimental investigation of the advantages and limitations of biopolymer, specifically xanthan gum (X.G.), to reduce susceptibility or prevent post-wildfire rain-induced hill-slope erosion. Water-repellency, or hydrophobicity, exists in minimal quantities in natural mineral forest soils but does not affect the soil cover permeability (DeBano, 1981; Doerr et al., 2000; Huffman et al., 2001). However, the hydrophobicity significantly intensifies when a wildfire vaporizes and condenses fuel-burn compounds into the surrounding soil. As a result, a newly post-wildfire formed surficial hydrophobic soil layer substantially reduces the infiltration of rainwater and promotes surface erosion (Crockford et al., 1991; DeBano, 1967, 1981; DeBano & Krammes, 1966; Doerr et al., 1996; Helvey, 1980; Huffman et al., 2001; Movasat & Tomac, 2020a, 2020b, 2020c, 2022a, 2022b; Savage, 1974; Scott & Van Wyk, 1990; Meeuwig, 1971). Furthermore, wildfire frequency has been exponentially rising. For example, in 2021, California (C.A.), U.S. had 8786 fires burning over 2.5 million acres, posing a threat of mudflows over burn scars following a fire (Department of Forestry and Fire, 2022). Mudflows in California, U.S., were triggered in 2021 with rain intensities as low as 8.89 mm/h (Department of Forestry and Fire, 2022).

X.G. reduces the permeability of sandy soils by filling pores (Gioia & Ciriello, 2006). For example, Ayeldeen et al. (2016) determined that sand's permeability coefficient decreased to 4 % of its original untreated value at 2 % X.G. concentration by weight after five weeks of curing. The longer the sand cures, the more permeability and hydraulic conductivity decrease as the X.G.-particle links change from a gel to thinner glass-like strands (Ayeldeen et al., 2016; Cabalar et al., 2017; Moghal & Vydehi, 2021). Besides decreasing permeability, biopolymer allows the soil to retain more water due to strong hydrogen bonding

* Corresponding author.
*E-mail address:* itomac@ucsd.edu (I. Tomac).

https://doi.org/10.1016/j.bgtech.2025.100180
Received 3 December 2024; Received in revised form 15 April 2025; Accepted 15 April 2025
Available online 17 April 2025
2949-9291/© 2026 The Authors. Publishing services by Elsevier B.V. on behalf of KeAi Communications Co. Ltd. This is an open access article under the CC BY license (http://creativecommons.org/licenses/by/4.0/).

(Khachatoorian et al., 2003). In addition, reduced permeability leads to soil-plugging effects, which aid in soil remediation (Khachatoorian et al., 2003). When looking for vegetation growth improvement in drylands, just 0.5 % X.G. implemented into the soil stimulates vegetation growth (Tran et al., 2019). The compressive strength of saturated, poorly graded Sydney sand and well-graded low-plasticity residual Piedmont soils mixed with X.G. increased (Lee et al., 2019; Soldo et al., 2020). For example, the compressive strength of the saturated residual Piedmont soil -SW-SM (well-graded sand with silt) increases from 181 kPa to 3348 kPa, 5989 kPa, and 6185 kPa for 1 %, 2 %, and 4 % X.G. concentration after five days of curing, with an initial water content of 16.5 % (Soldo et al., 2020). Dry blending mixes and coats the surface of the particles with the biopolymer, including clays or silicate nanocomposites (Alexandre & Dubois, 2000; Akin & Likos, 2016).

X.G. has been used in several studies to control and mitigate wind and water erosion on slopes. For example, Kavazanjian et al. (2009) conducted wind experiments using an aluminum conduit and a fan to expose biopolymer-treated sands to approximately 26 km/h airflow velocity. Applying an X.G. emulsion with a spray bottle lowered the soil loss percentage of experiments using 0.5 % X.G. concentration to 0.04 % from 32 % observed with untreated sand. Fly ash treated with 1 % X.G. remained undamaged, making it a suitable protective method against wind erosion, like previous work done by Chen et al. (2015), which determined mine tailings treated with biopolymers increased the penetration force. Movasat and Tomac (2020b) distributed a 4 % by weight ratio of X.G. to base hydrophobic sand, raining over it for 100 min and collecting overflown water and eroded sand every 10 minutes. They found that the water runoff generally increased in the XG-treated slopes while observing decreased soil erosion in the treated sand. Akin et al. (2022) drew the same conclusions for a slightly different setup, raining on the treated hydrophobic soil slopes sprinkled with 2.8 g of X.G. uniformly on a compacted soil surface for 30 min with a rain intensity of 102 mm/h, drying, and repeating the cycle two more times. Fly ash and overburden mine soil were stabilized against water erosion with as little as 1 % concentration of X.G., with similar results found by Joga and Varaprasad (2020) for two soil types in Karnataka, India. The more biopolymer formed, the soil is more resistant to shear stress and erosion, and the erodibility coefficient decreased from 9132 mm/h to 1120 mm/h as more dextran was produced (Ham et al., 2018). The decrease in the erodibility coefficient is due to the increase in shear strength from cohesion. Thus, a similar conclusion can be drawn for X.G. as Soldo et al. (2020) found that the cohesion increased by 3.2 after five days of curing.

Rainfall triggers the erosion of burned scars. An overview of recent rain types and intensities that led to post-wildfire debris flow reveals a wide range. For example, in 2018, in Montecito, CA, the highest average hourly rainfall intensity was slightly higher than 10 mm/h, with an instantaneous rainfall intensity jump to 50 mm/h a few minutes before the debris flow occurred (Tiwari et al., 2020). The cumulative rainfall over the three-day storm was around 37.5 mm. Oakley et al. (2017) synthesized post-fire debris flows from 19 precipitation events from 1980 to 2014 due to atmospheric rivers (A.R.s) and closed lows. A.R.s, defined as narrow regions of enhanced water vapor transport in the lower troposphere, can increase precipitation in mountain ranges at landfall (Ralph et al., 2016). Closed lows are low-pressure areas with a distinct center of cyclonic circulation that can completely encircle one or more height contours (Oakley & Redmond, 2014; NOAA, 2011). Within the 19 precipitation events studied, A.R.s were the atmospheric event for 11 out of 19, with the lowest rainfall range being 5–11 mm/h and 21 mm/h when observed over 15 minutes taking place in La Cañada Flintridge, CA, on December 12, 2009, within the Station burn scar. The highest average rainfall rate was 5–33 mm/h in San Bernardino, CA, on December 25, 2003, within the Grand Prix and Old Fire burn scars. Debris flows occurred within the Springs burn scar in the Santa Monica Mountains, CA, triggered by a 15-minute rain intensity of 15 mm/h on December 12, 2014 (Oakley et al., 2017).

Although previous studies showed the effects of biopolymers on improving sand shear strength and decreasing permeability, a limited number of studies use biopolymers as a post-wildfire slope mitigation technique, leaving much unknown, like, for example, a long-term perspective and exposure to environmental conditions and multiple variable rain events. Furthermore, little research focused on improving erosion by covering hydrophobic slopes with X.G. without exploring alternative application approaches. Therefore, this paper focuses on gaps in the literature regarding the effects of sand type and particle size, rain intensity, slope angle, and X.G. concentration, including the coupling of relevant parameters for mitigation of post-wildfire slopes, as well as the advantages and limitations of the method.

## 2. Materials and methods

This research's experiments and analysis systematically investigate the advantages and limitations of X.G.'s effectiveness for the remediation of hydrophobic sandy slopes. Among many biopolymer types that this study initially considered (gellan gum, agar, polyacrylamide, guar gum, chitosan, and alginate), X.G. (CASRN 11138–66–2) is selected as a representative biopolymer because it is widely available and commercially manufactured, bearing in mind that other researchers have studied the effects of differences between biopolymers on soil improvement. The experimental program includes investigating coupled effects of anticipated rain intensity, slope inclination, X.G. application technique, X.G. percentages, time, and environmental effects on susceptibility of erosion and erosion protection of fine, medium, and coarse sand.

### 2.1. Rainfall data collection

In addition to performing a literature review, we gathered real-time rain gauge data from two California post-wildfire debris flow events to design an appropriate range of rain intensities leading to post-wildfire erosion and debris flow. Monterey County and Silverado Canyon debris flow events provided more rain intensity data. In addition, the California Nevada River Forecast Center (CNRFC & NOAA, 2021) provides rain station precipitation maps and hourly precipitation summaries for their network. Fig. 1A shows the hourly rain intensities for the flow in Monterey County, CA, along River Road on January 27, 2021. The rain gauge station was within the River Fire burn scar, which burned on August 16, 2020. The debris flow onset correlates with the maximum hourly rainfall intensity of 8.89 mm/h at 4 a.m. PST on January 27 and 19.8 mm cumulative rainfall up to that time. However, as it began to rain again, the cumulative rainfall increased to 83.1 mm without further mudflows. Fig. 1B shows the flow data in Silverado Canyon, CA, in the last hour of January 28, 2021. The rain gauge station is within the Bond Fire burn scar, which burned for seven days from December 3–10, 2020. The maximum hourly rainfall intensity was 12.19 mm/h at 11 p.m. PST on January 27, and the cumulative rainfall after the storm was 39.4 mm. Despite higher rainfall intensity rates for 15-minute intervals, the average hourly rainfall intensity rates are consistent with those found during this research for various post-wildfire mudflows in late January 2021.

Natural rain events occurred during flume exposure to environmental conditions. Table 1 summarizes the nine R.E.s occurring from July 26, 2021, to December 26, 2021, with data courtesy of MesoWest from the University of Utah (https://mesowest.utah.edu/). Stations E3170 and F8273 are located 1.85 km and 3.27 km, respectively, from the experiment locations.

### 2.2. Experimental setups

Coarse, medium, and fine uniform sands are artificially hydrophobized with contact angles shown in Table 2 (Movasat and Tomac, 2020c; Movasat et al., 2023). The soil contact angle was determined

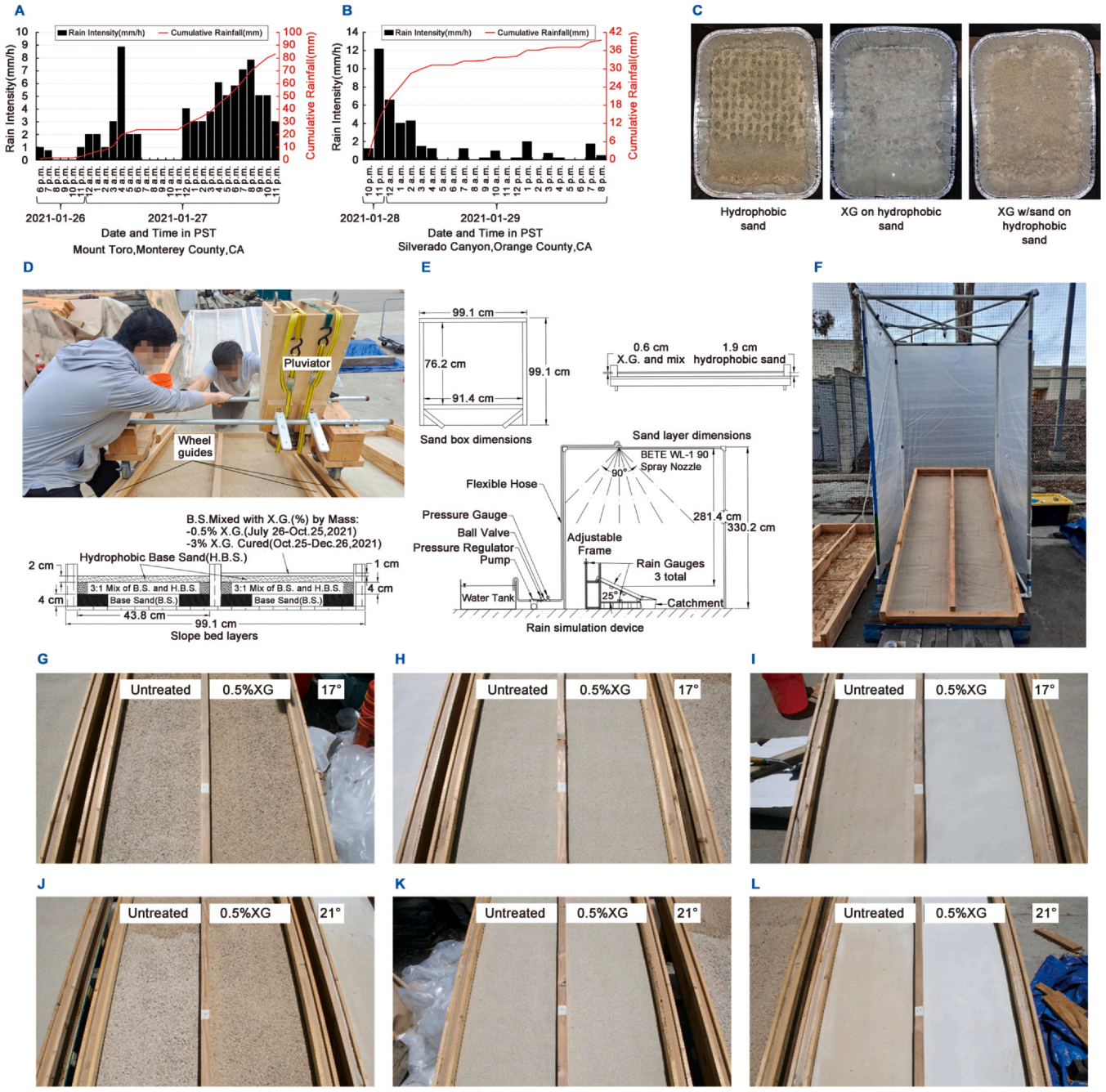



**Fig. 1.** (**A–B**) Mudflow-triggering rain intensities, January 2021 in California, U.S. in Monterey County along River Road and Orange County, Silverado Canyon; (**C**) The uniformity of the nozzle's spray pattern; (**D**) Environmental experiments consist of two parallel flumes for treated and untreated hydrophobic slopes sunbed pluviation; (**E**) Rainfall simulator setup with a sandbox, adjustable frame, eroded material and water catchment, frame to hold the rain nozzle, water tank, water pump with a pressure regulator, and a pressure gauge; (**F**) Experimental setup; Six prepared double beds: (**G**,**J**) Coarse sand, (**H**,**K**) Medium sand, (**I**,**L**) Fine sand.

using the sessile drop method. Phantom Miro C320 high-speed scientific camera records videos at 1500 fps and 1280 × 1024 pixels. Therefore, the sessile drop technique proposed here ensures a good baseline for measurements at different substrates and sufficiently minimizes image exposure (Saulick et al., 2017). The water drop penetration test classifies the sand as severely hydrophobic for each batch. First, the sand is submerged in a 90 % Reagent Grade 100 alcohol and 10 % triethoxy-n-octylsilane solution by volume for 48 h, mixing the sand after one day. After this, the submerged soil is washed to remove any reactive compounds and oven-dried for 24 h.

Controlled-rain experiments use custom-built setup. Fig. 1E shows a 99.1 cm by 99.1 cm box made of wood and plywood with wheels for easy manipulation. The inner dimensions are 91.4 cm by 76.2 cm, with a 1.9 cm high wood plank allowing water and superficially eroded material collection. Angled barriers guide sand and water runoff into a catchment at the bottom of the slopes. A zinc-plated slotted angle frame connected with nuts and bolts supports the experiment box and adjusts the slope. A suitable rain simulation system reaches the target values after finding appropriate rain intensity values for storms that triggered post-wildfire mudflows. Modifying the system of Carvalho et al. (2014), a 330.2 cm tall supporting frame supports the hose and spray nozzle at the top. Calibration of different spray nozzles and pressures enables the physical modeling of the higher rain intensity values for reported events measured within 15-minute intervals, such as the reported 15 mm/h in

**Table 1**
Data and slope treatment type for each rain event courtesy of MesoWest from the University of Utah (https://mesowest.utah.edu/).

| RE | Date | Station ID | Duration (min) | Avg. *i* (mm/h) | Max. *i* Time (PST) | Max. *i* (mm/h) | Treatment Type |
|---|---|---|---|---|---|---|---|
| 1 | 2021-07-26 | E3170 | 75 | 0.76 | 4:45–5 a.m. | 2.03 | U |
| 2 | 2021-08-11 | E3170 | 31 | 0.49 | 4–4:31 a.m. | 0.49 | U |
| 3 | 2021-09-09 | E3170 | 29 | 5.78 | 8:02–8:17 p.m. | 9.14 | U |
| 4 | 2021-09-27 | E3170 | 464 | 0.29 | 6:01–6:15 a.m. | 1.09 | U |
| 5 | 2021-10-05 | F8273 | 435 | 1.40 | 1:31–1:46 a.m. | 4.06 | U |
| 6 | 2021-10-08 | F8273 | 225 | 1.02 | 4:46–5:01 a.m. | 3.05 | U |
| 7 | 2021-10-25 | F8273 | 151 | 1.69 | 4:31–4:46 p.m. | 11.18 | U |
| 8 | 2021-12-14 | E3170 | 750 | 2.84 | 12–12:15 p.m. | 14.22 | C |
| 9 | 2021-12-26 | E3170 | 166 | 1.52 | 2:31–2:45 a.m. | 14.15 | C |

Note: RE = rain event; *i* = rain intensity; U = uncured 0.5 % XG; C = cured 3 % XG

the Santa Monica Mountains, CA, and 50 mm/h in Montecito, CA. For example, at a water pressure of 241.3 kPa, the HH-4.3 W nozzle with a 120° spray angle from Spraying Systems Co. gives the lower 15-minute rain intensity of 15 mm/h with a typical natural raindrop sizes diameter range of 0.55–3.0 mm and an average drop size diameter of 1.6 mm (Law et al., 2021; Martner et al., 2008; Nanko et al., 2006), and a BETE WL-1 90 nozzle with a 90° spray angle gives a 15-minute rain intensity of 50 mm/h with the same drop size ranges. Drop sizes were estimated from the footage of high-speed cameras. The height of the spray nozzle is determined by estimating the terminal drop velocity height for a 3-mm drop size using van Boxel's (1997) equations (Movasat et al., 2023). BETE-WL1 full cone nozzle with a 90° spraying angle was tested for spatial uniformity by locating four rain gauges in the testing area with promising results within the scope of our previous research, and we did not see any significant deviations from uniformity through the spray range available using our pumps in the laboratory setup (Movasat & Tomac, 2025). The rain intensity is measured with two rain gauges on either side of the experiment box and one at the top of the adjustable frame during the calibration and later for each experiment. On level ground, the hydrophobic sand uniformly fills the sandbox up to a height of 1.9 cm. Different setups investigate an optimal erosion control: (1) control setups with untreated hydrophobic sand, (2) setups with dry X.G. and sand mix pluviated over the hydrophobic layer, (3) dry X.G.-sand mix, which was sprayed with water at 16.5 % layer's mass, or 371.25 g and allowed to cure for 24 h before raining experiments. Then, the adjustable frame is set at the target angle's height, and the sandbox is rolled over carefully and gently placed at the angle. The total used mass for the X.G. sand mix is 2250 g, adjusted for each experiment, with a maximum of 3 % X.G. and 97 % base sand by mass.

Experiments exposed to a natural environment, such as tree debris, animal interactions, and multiple occurrences of natural rainfall. A total of six slope beds are created out of wood, two beds for each sand type angled at $\alpha = 17^{\circ}$ and $\alpha = 21^{\circ}$ (Fig. 1D, F, G–L). Each bed was made to have two flumes with inner dimensions of 43.8 cm in width and 182.9 cm in length. Measuring through critical surface tension, Huffman et al. (2001) found soil hydrophobicity on wildfire-burned slopes to be stronger at the surface and dissipate as the depth increases, with the last relevant depth further analyzed being 6 cm. According to these findings, the flumes were pluviated, as seen in Fig. 1D, with the hydrophobic sand and a mix of hydrophobic and hydrophilic sand layers, as seen in Fig. 1D, to mimic the natural soil hydrophobicity decrease with depth. Yellow straps on our pluviation device allow for adjustment of the height of the pluviator concerning the surface. As the surface is raised, the height is adjusted so that the drop height is always constant to achieve a uniform sand density. Calibration tests were performed in a mold to achieve loose relative densities applicable for surface soils of 20 %–22 %; using a small drop height of up to 20 cm was sufficient. The proposed approach approximates a more heterogeneous natural environment. A roller system and wheel guides with a horizontal support system allowing sliding ability are created to keep a constant drop height while pluviating the sands. The bottom of the slopes contains a wood barrier to support the bottom layers while allowing the top layers with hydrophobicity and the X.G. treatment to be collected in a catchment for erosion and water overflow measurements after rain events. Depending on the sand type, rainfall-induced infiltration and surface runoff properties may differ. The top layer of the left flume on each slope bed contains unmitigated hydrophobic sand, while the right flume has the X.G. treatment. Initially, the hydrophobic base sand on the right flume of each slope bed was covered with 1 cm of the base sand mixed with 0.5 % X.G., which was used on the first seven rains (Fig. 1G–L). On November 21, 2021, the treated slopes were recovered using 3 % concentration by mass of X.G. mixed with the base sand and cured immediately after spraying the layer with 16.5 % mass of water, forming a hardened crust layer after drying.

Throughout the experiment, leaves, twigs, and bark from the surrounding trees landed on the slopes, and a family of raccoons occasionally stepped on the slopes. With all these external factors commonly occurring in nature, these experiments paired with natural rain events (RE) provide results for the real-world performance of hydrophobic slopes post-treatment for coarse, medium, and fine sand.

## 3. Results and discussion

### 3.1. Rain simulator experiments-based water runoff and sand erosion susceptibility

The experiment with a laboratory-controlled raining system from nozzles on artificially hydrophobic flumes consists of experiments with

**Table 2**
Soil contact angle and particle grading parameters measured with the sessile drop method.

| Soil | Contact angle (°) | | $C_u$ | $C_c$ | $D_{10}$ (mm) | $D_{50}$ (mm) | $D_{60}$ (mm) |
|---|---|---|---|---|---|---|---|
| | Hydrophilic | Hydrophobic | | | | | |
| Fine | 60 | 115 | 1.50 | 0.90 | 0.15 | 0.2 | 0.23 |
| Medium | 38 | 100 | 1.67 | 1.01 | 0.28 | 0.4 | 0.47 |
| Coarse | 27 | 96 | 1.53 | 1.03 | 0.46 | 0.65 | 0.70 |

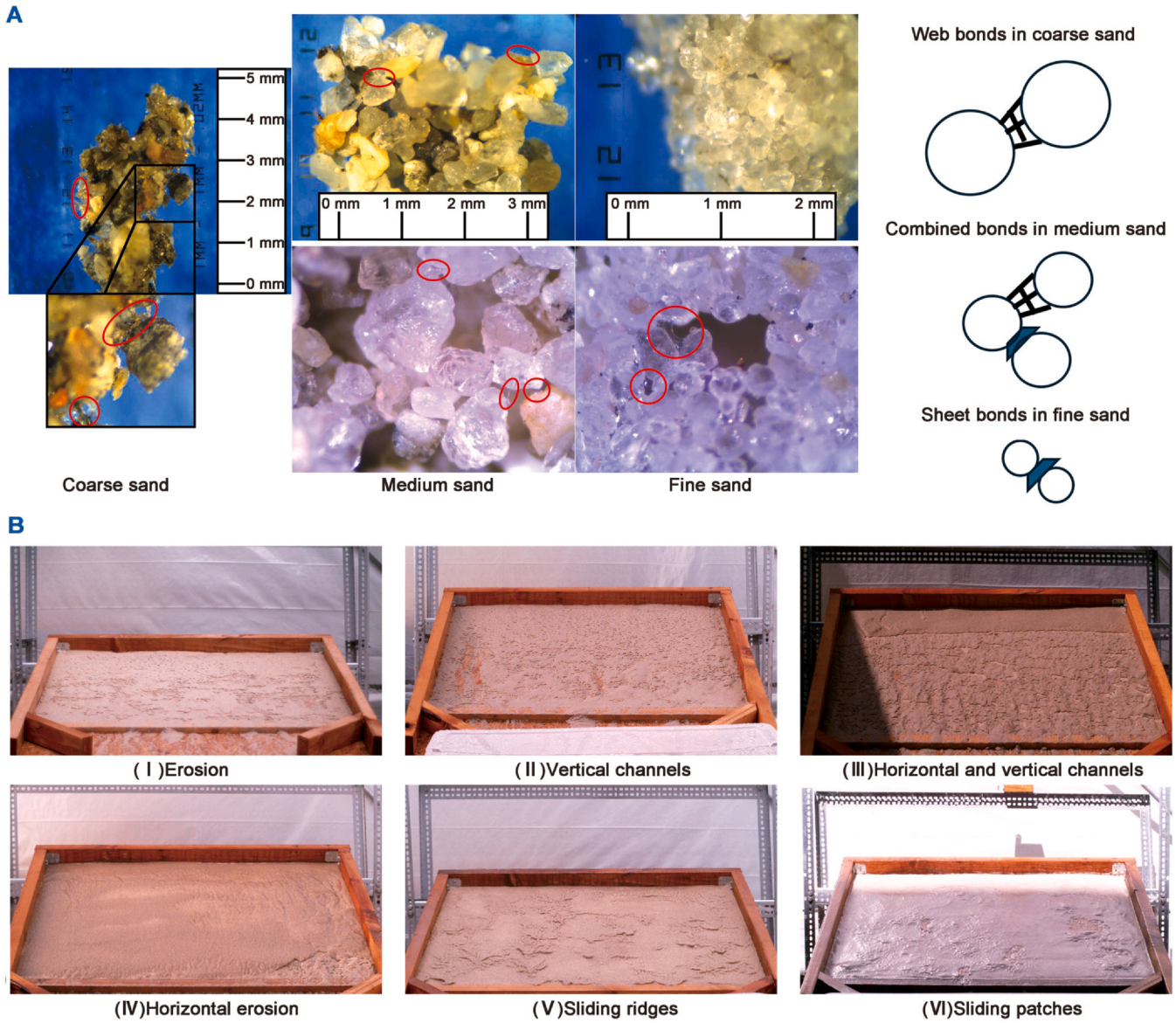



**Fig. 2.** (**A**) Microscopic images of cured 3 % X.G. crust bonds in the coarse, medium and fine sand; (**B**) Observed erosion types.

varying slope angles and rain intensities and exploring optimal design for X.G. applications. Preparatory experiments use 50 mm/h rain intensity on untreated hydrophobic surfaces and provide the erosion baseline for 10°, 15°, 20°, and 25° slopes for medium sand and 10°, 25°, and 30° for fine sand.

*3.1.1. Bonding mechanisms between X.G. and hydrophobic sand particles*

Sprinkling X.G. on the surface of hydrophobic sand slopes was initially considered, but indoor, small-scale experiments with an identical rain simulation device from Carvalho et al. (2014). Results showed multiple unfavorable crater-like ridges from raindrop impacts. Although the X.G. sprinkling method seemed to aid in erosion resistance at first, the surface layer soon became over-wetted during the trial of 15 min of rain, and the whole swollen X.G. layer excessively deformed and failed. Thus, covering the sand surfaces with an uncured XG-sand layer increases the risk of failure for prolonged rain events.

Therefore, raining experiments are proposed on sand slopes sprinkled with an uncured and cured mix of X.G. and hydrophilic sand. When treated with sprinkling water, the X.G. treated soil layers solidify, as shown in the study by Soldo et al. (2020). Microscopic images of pieces of naturally re-dried crusts (Fig. 2A) prove the proposed concept, showing the absence of deformation from each sand type and different styles of X.G. bonding in each sand. Fig. 2A shows that in the coarse sand, X.G. bonds are web-like, with very tiny particles attached to them as the strands span from one large particle to another. The bonds encapsulate the particles completely in the fine sand, almost sheet-like, as seen in Fig. 2A. The medium sand crust bonds seem to be a combination of the other two-crust bonds, with X.G. strands spanning from particle to particle, with an addition of inter-particle close contact cementing bonds.

*3.1.2. Surface morphology evolution of X.G. treated surfaces during raining*

Overall, most X.G. treated surfaces successfully reduce erosion and, in some cases, show stability or minor erosion compared to untreated hydrophobic sand plastic deformation. However, several experiments treated with X.G. gradually developed non-favorable surface morphologies that enhance erosion or water overflow. Fig. 2B shows erosion types based on various test conditions, such as slope angle and X.G

**Table 3**
Surface erosion type and runoff data for cured X.G. experiments at 15 mm/h rain.

| Tests | X.G. (%) | Rain Duration (min) | Surface Erosion Type | Normalized Runoff | | Eroded (%) |
|---|---|---|---|---|---|---|
| | | | | Water (mL/cm$^2$) | Soil (mg/cm$^2$) | |
| 25° | | | | | | |
| Fine | 1 | 15 | Fig. 2B(V) | 0.02 | 0 | 0 |
| | 1 | 30 | Fig. 2B(V) | 0.07 | 0 | 0 |
| | 3 | 15 | Fig. 2B(V) | 0.24 | 0 | 0 |
| | 3 | 30 | Fig. 2B(V) | 0.38 | 0.002 | 0.06 |
| Medium | 1 | 15 | Fig. 2B(V) | 0.14 | 0 | 0 |
| | 1 | 30 | Fig. 2B(I) | 0.29 | 0.002 | 0.09 |
| | 3 | 15 | Fig. 2B(V) | 0.04 | 0 | 0 |
| | 3 | 30 | Fig. 2B(VI) | 0.05 | 0 | 0 |
| Coarse | 3 | 15 | Fig. 2B(V) | 0.24 | 0 | 0 |
| | 3 | 30 | Fig. 2B(V) | 0.54 | 0 | 0 |

Note: All experiments were successful, with little to no erosion.

content, and classifies surface erosion morphology into six different types. Tables 3 and 4 summarize experimental results and erosion types, including those without visible surficial changes. For example, Fig. 2B(I) shows rain erosion of untreated hydrophobic medium sand at a 15° slope. The sand surface slowly erodes under the impact of the raindrops, and the erosion increases. Similar morphology evolves at the 10° and 15° medium and 10° for fine sand slopes under higher rain intensity. Finally, preferential surficial flow channels lead to significant erosion at steep 20° and 25° untreated slopes (Fig. 2B(II)). Two instances of extreme surface morphology occur in an uncured mix of 0.5 % X.G. and medium sand at the 20° and 25° angles, as seen in Fig. 2B(III). First, large horizontal sections slide down as the uncured mix had no solidified bonds while containing little X.G. Subsequently, the exposed hydrophobic sand develops channels like the untreated slopes at these same angles. By increasing the concentration of X.G. in the mix with medium sand, for example, to 3 %, the horizontal erosion effect persists, but at a significantly smaller scale without channels (Fig. 2B(IV)). Fig. 2B(V) shows sliding of approximately 50 % surficial ridges observed over the sand and sprinkled with water and cured for 24 h. Curing produces a crust with solid bonds between the particles (Fig. 2A) and less erosion. As a result, small ridges form under raindrops that impact different surface sections, then attempt to slide down while

**Table 4**
Surface erosion type and runoff data for cured X.G. experiments at 50 mm/h for 15 min.

| Tests | X.G. (%) | Test Type | Surface Erosion Type | Normalized Runoff | | Eroded(%) |
|---|---|---|---|---|---|---|
| | | | | Water (mL/cm$^2$) | Soil (mg/cm$^2$) | |
| 10° | | | | | | |
| Fine | 0 | N | Fig. 2B(I) | 1.14 | 46.05 | 2.52 |
| | 3 | C | None[a] | 1.62 | 0 | 0 |
| Medium | 0 | N | Fig. 2B(I) | 1.06 | 37.31 | 2.42 |
| 15° | | | | | | |
| Medium | 0 | N | Fig. 2B(I)[c] | 0.16 | 78.45 | 4.68 |
| | 3 | C | Fig. 2B(V)[a] | 1.15 | 0.3 | 0.01 |
| 20° | | | | | | |
| Fine | 3 | C | Fig. 2B(V)[a] | 0.02 | 0.0004 | 0.02 |
| Medium | 0 | N | Fig. 2B(II) | 0.26 | 73.31 | 3.84 |
| | 1 | N | Fig. 2B(III) | 0.73 | 376.33 | 14.79 |
| | 3 | C | Fig. 2B(V)[a,c] | 1.15 | 0.32 | 0.01 |
| Coarse | 3 | C | None[a] | 0.23 | 0.64 | 0.02 |
| 25° | | | | | | |
| Fine | 0 | N | Fig. 2B(II) | 0.69 | 325.26 | 16.59 |
| | 1 | C | Fig. 2B(VI)[a,c] | 0.62 | 1.327 | 0.05 |
| | 2 | C | Fig. 2B(VI)[a] | 0.74 | 229.93 | 8.86 |
| | 3 | C | Fig. 2B(V)[a] | 0.1 | 0.95 | 0.03 |
| Medium | 0 | N | Fig. 2B(II)[c] | 0.59 | 57.96 | 3.46 |
| | 3 | N | Fig. 2B(IV)[a,c] | 0.35 | 69.99 | 2.1 |
| | 3 | ND | Fig. 2B(VI)[a,b] | 0.64 | 1.58 | 0.05 |
| | 1 | C | Fig. 2B(V)[a,b] | 0.4 | 0 | 0 |
| | 3 | C | Fig. 2B(VI)[a] | 0.23 | 1.27 | 0.04 |
| Coarse | 2 | C | Fig. 2B(V)[a,b] | 0.26 | 0.12 | 0.01 |
| | 3 | C | Fig. 2B(V)[a] | 0.26 | 0 | 0 |
| 30° | | | | | | |
| Fine | 0 | N | Fig. 2B(II) | 0.6 | 1446.08 | 65.83 |
| Medium | 1 | N | Fig. 2B(III)[c] | 0.79 | 531.97 | 21.82 |

Note: N = not cured; N.D. = one day after the corresponding N test; C. = 24 h cured.
[a] successful in reducing erosion compared to untreated hydrophobic slopes.
[b] shown in Fig. 2B.
[c] used as a reference picture in Fig. 3.

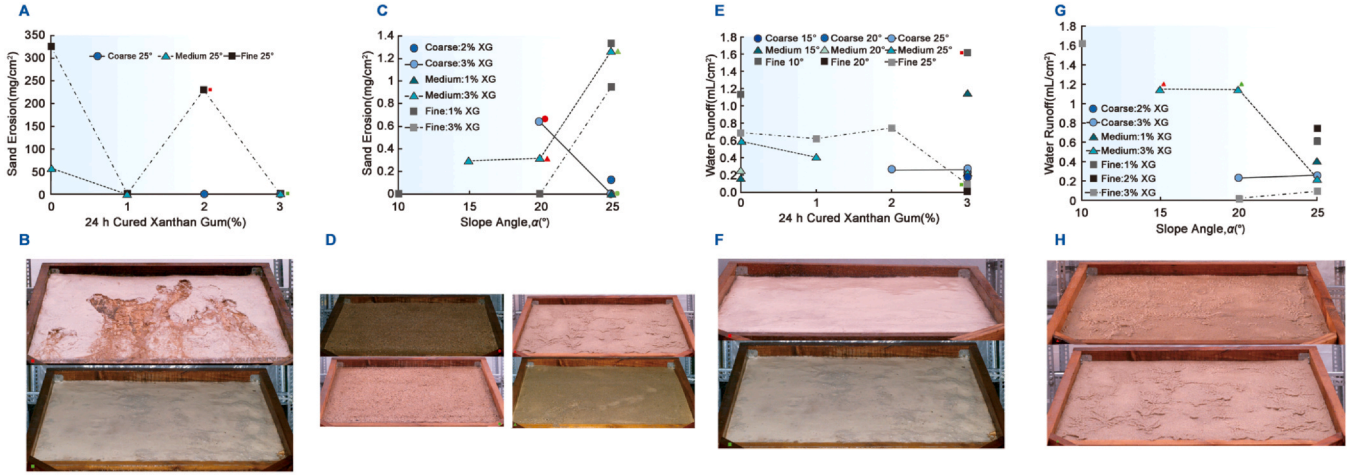



**Fig. 3.** Sand erosion vs. slope angle for 24 h cured X.G. at 50 mm/h rain intensities: (**A**) Corresponding symbol and colors for reference image data points; (**B**) 24 h cured fine sand at 25°, Top: 2% XG, Bottom: 3% XG; (**C**) Corresponding symbols and colors for reference image data points; (**D**) 24 h cured 3% XG coarse sand, Top: 20°, Bottom: 25°(left), 24h cured 3% XG medium sand, Top: 20°, Bottom: 25°(right). Water runoff vs. X.G. percentage and slope angle for varying 24 h cured X.G. percentages: (**E**) Corresponding symbol and colors for reference image data points; (**F**) 24 h cured 3% XG fine sand, Top: 10°, Bottom: 25°; (**G**) Corresponding symbol and colors for reference image data points; (**H**) 24h cured 3% XG medium sand, Top: 15°, Bottom: 20°.

the rest of the crust holds in place. While cured, coarse sand slopes with a mix of 2 % and 3 % X.G. at 25°, medium sand experiments with 1 % X.G. at 25° and 3 % X.G. at 15° and 20°, and fine sand slopes with 3 % X.G. at 20° and 25° all experienced the morphology type in Fig. 2B(V). Fig. 2B(VI) shows a morphology characterized by individual sliding patches formed when the bonds from the cured X.G. were not strong enough to hold the sliding sections in place. For example, individual sliding patches occur in the medium sand with a mix of 3 % X.G. at the 20° to 25° slopes and fine sand with 1 and 2 % X.G. at a 25° slope, while 3 % X.G. prevents sliding patches of fine sand. In addition, while the not cured mix of 3 % X.G. develops horizontal erosion when allowed to cure by re-drying and to test again the day after, a tiny sliding section develops.

Table 3 summarizes observations of surface morphology at a lower rain intensity of 15 mm/h, which overall show more favorable results. Coarse and fine sands with different cured X.G. percentage mixes formed small ridges after 15 min, with little to no changes after another 15 min, not affecting the overall erosion trends. For cured medium sand, visual surface assessment of 1 % and 3 % X.G. develop very few ridges after 15 min. However, after another 15 min, another surface erosion type occurs, where a small patch begins to slide down the slope for the mix of 1 % X.G. Furthermore, at this lower rain intensity, an uncured blend of 0.5 % X.G. does not develop the extreme horizontal erosion and channels, but only the horizontal erosion at the smaller scale, much like the uncured 3 % X.G. at the higher intensity. Swelling of ridges and surfaces upon wetting can enhance water-holding capacity to a small extent.

### *3.1.3. Water runoff and erosion of X.G. treated surfaces during raining*

The amounts of collected sand normalized by the experiment surface area are plotted against the X.G. percentage in the mix and the slope angle in Fig. 3 to understand erosion better. The overall trend indicates that X.G.'s percentage increases better stabilize slopes, and more X.G. is needed at higher angles and finer sands. Furthermore, erosion susceptibility in treated fine sands is problematic due to the random development of unfavorable surface morphologies. For example, Fig. 3A–B show that although most experiments at 1 %–3 % XG-sand mix cured for 24 h develop different levels of sliding ridges, the measured erosion is still significantly reduced compared to the hydrophobic sand experiments. However, fine sand with 24 h cured 2 % X.G. at 25° performs poorly (Fig. 3). Top Fig. 3 at 25° shows how the compromised cured protective layer above the hydrophobic sand as a piece of the crust breaks. The water that continuously rains and flows down the slope chips away pieces at the exposed location, increasing the size of the sliding patches. From the slope angle perspective, slopes above 20° enhance erosion in cured XG-sand, including all fine sands regardless of the X.G. percentage, and medium sand with 3 % X.G. Furthermore, exciting connections exist between the observed surface morphology and erosion rates. The coarse sand runoff at a 20° slope was 0.64 mg/cm$^2$, while the 25° slope yielded no collected erosion.

The 20° coarse slope experienced no unusual surface morphology, while the zero-erosion 25° slope formed ridges (Table 3). Unlike a whole section pulling down and forming ridges, tiny particles break out of X.G. bonds and roll, leading to no sliding ridge formation. Also, while the collected erosion was higher at the 20° than the 25° slope, it was only 4.16 g, an amount of no concern. The same phenomenon is seen with medium sand at a 25° angle using a mix of 1 % X.G. the surface forms sliding ridges and collects no erosion. Fig. 3 also shows that the medium and fine sands follow a parallel trend, increasing the collected sand runoff by 0.95 mg/cm$^2$ when changing the slope from 20° to 25°, also connected to the surface morphology. Many sliding ridges form on the medium sand experiment with less erosion than coarse sand. The surface morphology changes at the same angle that the coarse sand experiences a shift from sliding ridges to sliding patches. Though fine sand does not develop ridges throughout most of its surface, a tiny patch erodes at the bottom right of the slope. Ridge development allows less sand runoff because sand particles that roll downhill now have a more potent cohesive force from the cured X.G. However, after continued rain at high intensities, the stronger crust bonds turn from solids to gooey, and the ridges risk evolving into sliding patches. Based on this, curing a sand mix with 3 % X.G. and developing ridges decreases the amount of sand runoff but can lead to sliding patches and elevated erosion.

Fig. 3E–H show that water runoff remains roughly the same at untreated to 1 % X.G. as the surfaces formed vertical channels and sliding patches, slightly increasing at 2 % X.G. as the surface develops large sliding patches. Furthermore, the water runoff decreases sharply between 2 % and 3 % X.G. for fine sand once the surface forms small sliding ridges. The lowest water runoff occurs at 25° and cured 3 % X.G. sand mix over coarse, medium, and fine sand slopes. Fig. 3E–H also show examples of surface morphology for fine and medium sand slopes with 3 % X.G. The

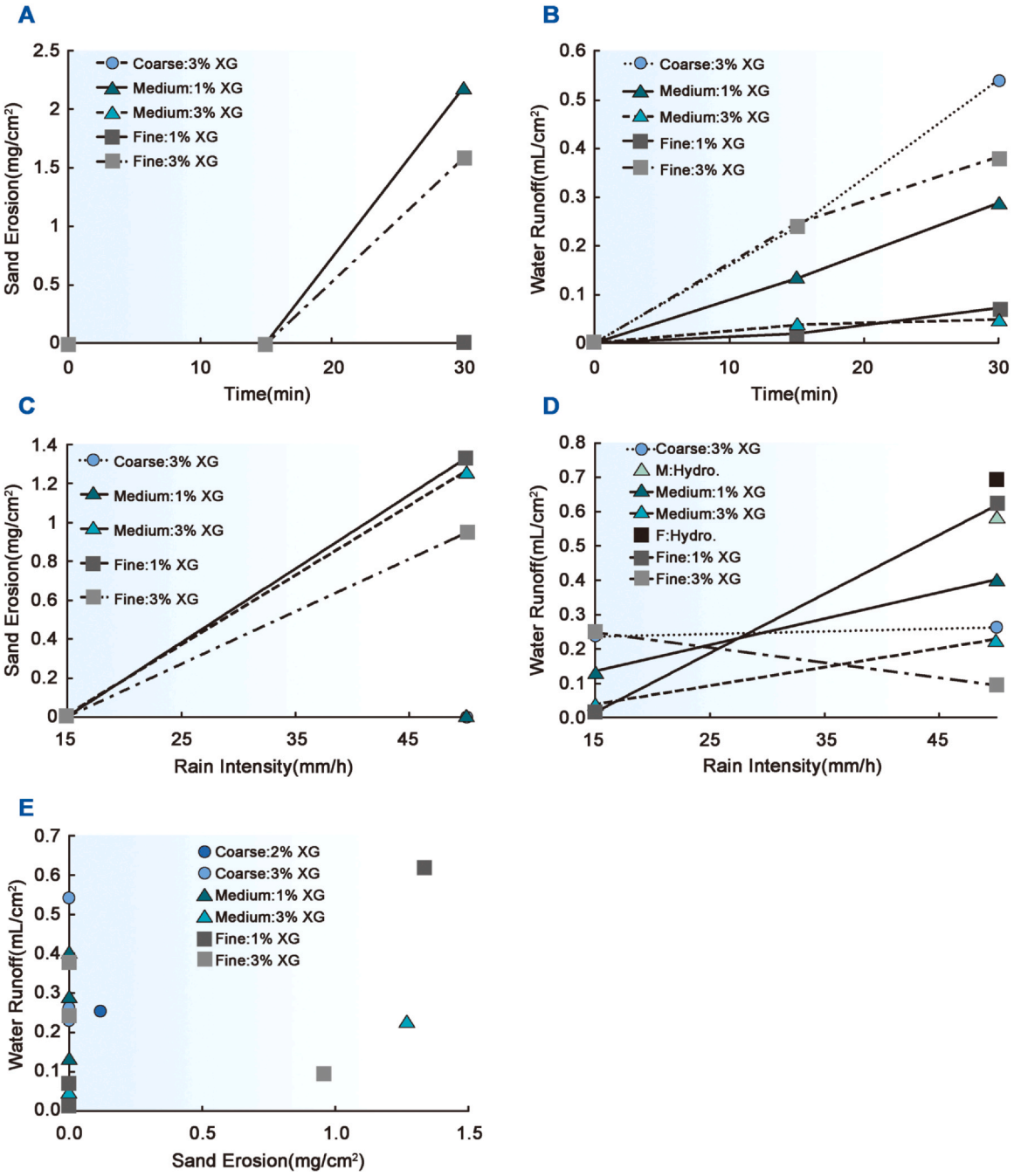



**Fig. 4.** Water runoff and sand erosion with time for 15 mm/h rain intensities, and vs. rain intensity, water runoff with sand runoff for 24 h cured X.G. percentages at a 25° angle.

10° fine sand slope has no surface morphology changes and yielded a much higher water runoff, while the 25° slope has small sliding ridges and experienced a reduced water runoff. Coarse and fine sand experiments show a slight water runoff increase with an increasing slope, regardless of sand erosion. At a 25° slope, there are coarse, medium, and fine sand trials with cured X.G. percentages with no or little erosion and a water runoff range of 0.02 mL/cm$^2$ to 0.73 mL/cm$^2$. Most of these no-erosion data points are below 0.30 mL/cm$^2$. To conclude, although the water runoff can be high without erosion, water and sand runoff increase exponentially once the erosion starts.

Rain duration changes surface morphology, erosion, and water runoff. Fig. 4 shows that the water runoff for the lower rain intensity of 15 mm/h remained consistent with little change in slopes for the duration of the experiment.

The higher the X.G. percentage, the lower the water runoff for cured medium sand. For cured fine sand, the higher the X.G. percentage, the higher the water runoff, and the more water runoff comes from cured coarse sand with 3 % X.G. Fig. 4 shows the sand and water erosion trends as the rain intensity increases from 15 mm/h to 50 mm/h at the steepest slope of 25°. The tested X.G. percentages for each sand show no sand erosion at 15 mm/h low rain intensity. At the higher rain intensity of 50 mm/h, 3 % X.G. controls erosion better than the 1 % counterparts overall, except for the experiment in medium sand. Furthermore, 3 % X.G. overall shows less water runoff sensitivity to rain intensity, although there are some variations between sands. Interestingly, cured fine sand with 1 % X.G. has the lowest water runoff at lower rain intensities but increases the most as the rain intensity increases, indicating high erosion potential to turn catastrophic in fine sands, even

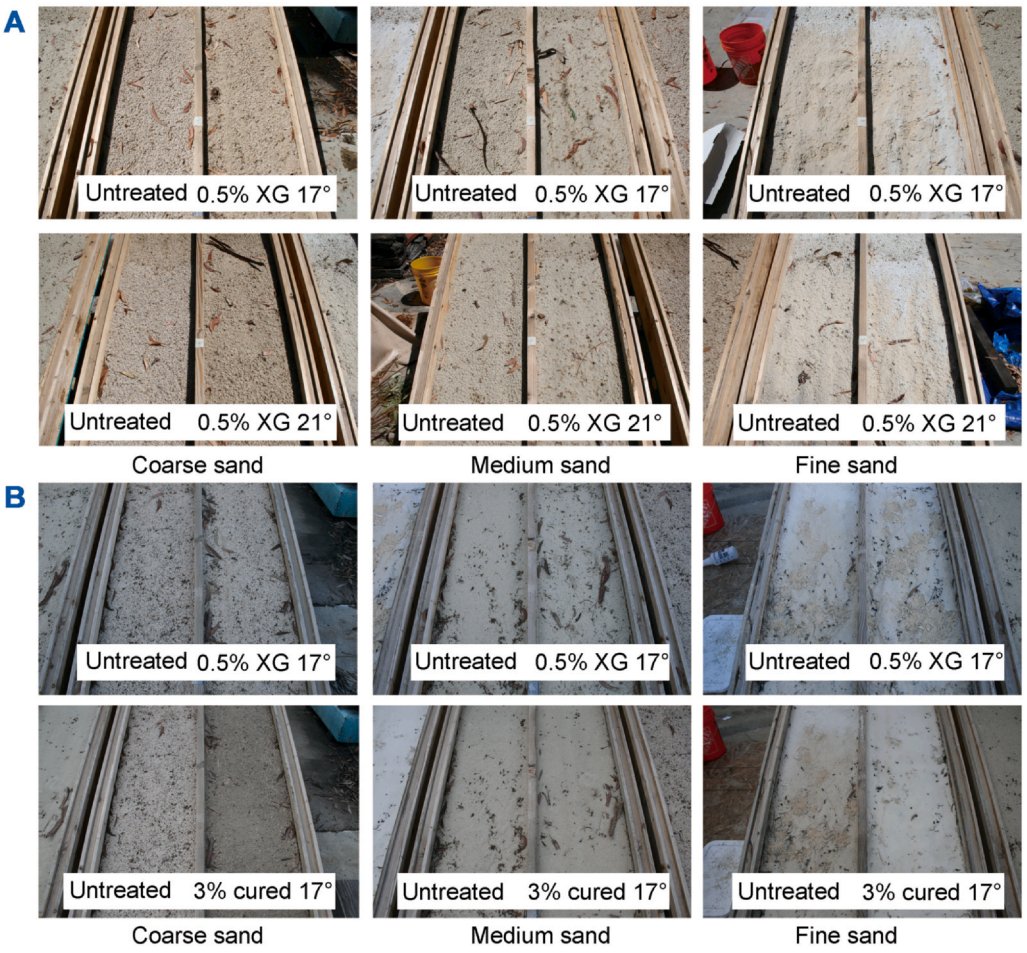



**Fig. 5.** Surface morphology evolution for slopes exposed to environmental conditions: (**A**) Surface morphology after RE 3 on September 10, 2021; (**B**) 17° slopes before (*top*) and after (*bottom*) re-covering (November 22, 2021).

when improved with X.G. Finally, cured coarse sand with 3 % X.G. is relatively insensitive to rain intensity.

### *3.2. Long-term water runoff and erosion in slope flumes exposed to the environment*

Parallel flumes with hydrophobic and treated fine, medium, and coarse sand surfaces were exposed to environmental conditions on the UC San Diego campus for approximately six months during the rainy season. Table 1 shows real-world rainstorms are uncontrolled events with varying average rain duration and 15-minute peak rain intensities.

#### *3.2.1. Surface morphology evolution over six months*

The first two R.E.s did not cause significant changes to the slopes as the rain durations were short and the rain intensities were low (Table 1). Although uncured when originally applied, the initial rain from RE 1 wetted the X.G., coating the sand particles and forming a hardened crust layer after drying, much like the cured treatment process applied after the seventh RE. After RE 2, raccoons walked over the surface of the treated coarse and the untreated fine slopes at 17°. The treated coarse sand was not primarily affected, but the untreated fine sand contained a section of the displaced hydrophobic layer, exposing the less hydrophobic layer beneath.

However, this did not affect the overall erosion trends, as the 17° fine slopes data reveal that the 0.5 % X.G. flume still experienced higher erosion than its untreated counterpart during RE 3. RE 3 with a max. 15-minute rain intensity of 9.14 mm/h caused the first significant change in surface morphology, leading to a larger erosion yield for each slope and sand type. Fig. 5A depicts the increase in surface morphology when comparing the sand types, with the minor change being in the coarse slopes, some channels beginning to form on the medium slopes, and deep channels already formed on the fine slopes. As the rain events continued, the channels seen in the fine sand slopes became more prevalent, with extensive channels (Fig. 5B, Fig.6). With a cured layer from the X.G. after continuous rain, more raccoon activity broke apart the surface layer and created more drastic surface conditions, exposing the hydrophobic layers susceptible to mudflows (Fig. 5B).

#### *3.2.2. Water runoff and sand erosion during nine natural rain events over six months*

In Fig. 6, comparing these images before re-covering with their corresponding surface morphology after RE 8, the erosion followed the same pattern, with most of the flow diverting into the pre-formed channels and chipping away the cured layer at those sections. Fig. 5 and Fig. 6 also show the state of the slopes during the last two R.E.s. The surface morphology was not the only factor that led to enhanced erosion, as Fig. 5B and Fig. 6A reveal that the X.G. treated flume had still not dried seven days later, three days before RE 9, with a rain intensity of 14.15 mm/h and a rain duration of 166 min, due to the higher X.G. percentage and the colder temperature observed in December. With the slopes over-wetted, the hardened crust layer remained in a gel state, allowing entire sections along the pre-existing channels to erode swiftly. Fig. 6B shows the final surface morphology of each slope.

Because the raining variables change from one storm to the following, erosion and water runoff may be assumed not to follow a trend. However, when plotting the 15-minute peak rain intensities against

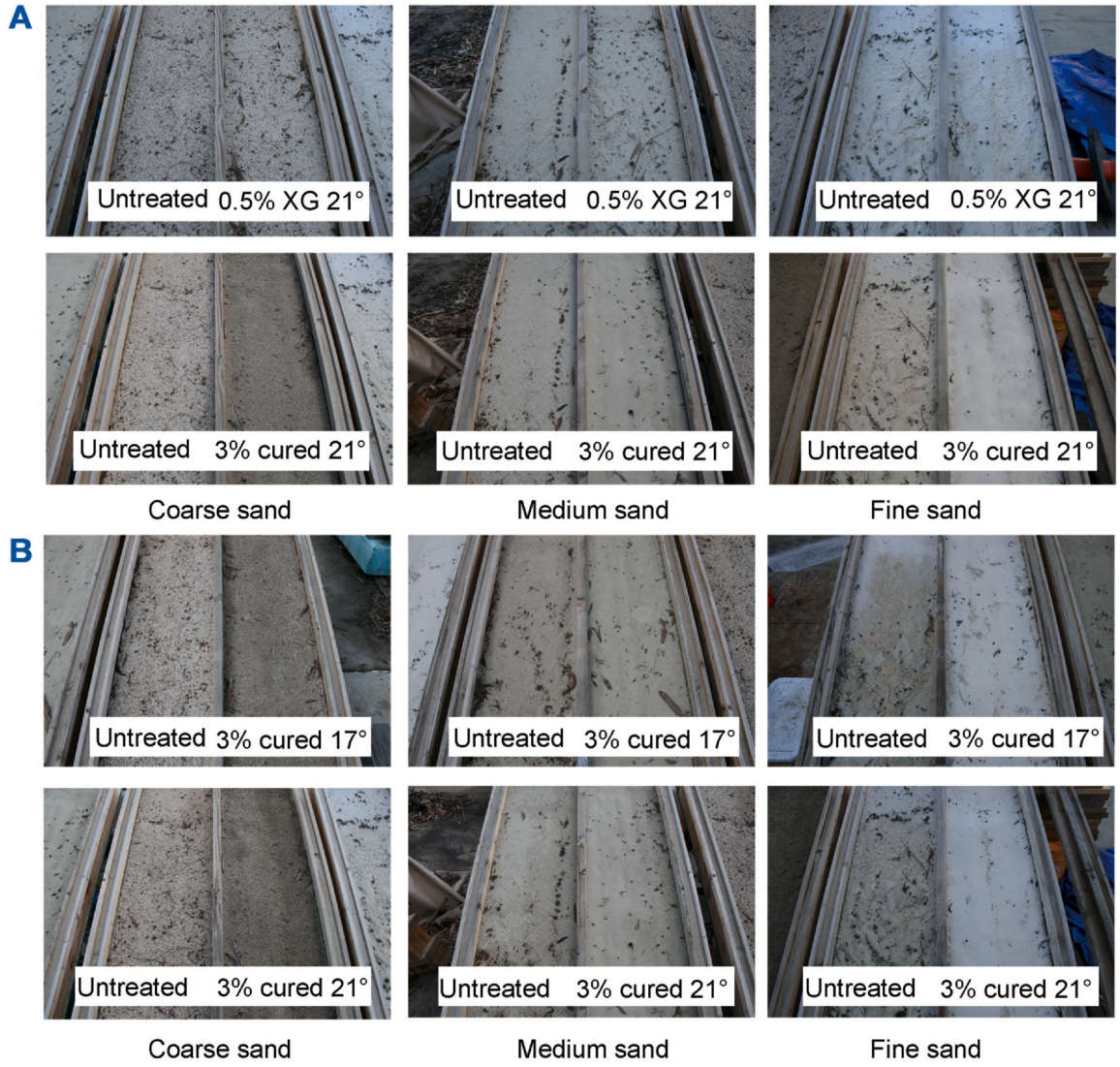



**Fig. 6.** Surface morphology evolution for slopes exposed to environmental conditions: (**A**) 21° slopes before (*top*) and after (*bottom*) re-covering (November 22, 2021); (**B**) Final surface morphology on February 4, 2022.

erosion and water runoff (Fig. 7), they both follow the trend of the rain intensities regardless of the duration it rained. However, this ceases to be the case after the slopes are re-covered. As for the treatment performance, Fig. 7A–B show that the 0.5 % X.G. treated fine sand flumes did not reduce erosion compared to the untreated slopes, with the angles 21° and 17° eroding even more for RE 3 and RE 5, respectively. On these same R.E.s, the water runoff for the treated flumes was also slightly more than observed for the untreated slopes. Once re-covered with the cured 3 % XG-sand mix, the 17° treated slope performed much better, with 28.31 mg/cm$^2$ eroded as opposed to 120.31 mg/cm$^2$ from the untreated flume during RE 8. The 21° treated slope performed slightly better than its untreated counterpart when re-covered and cured with 3 % X.G. The final RE saw a significant increase in erosion and water runoff for the XG-covered slopes due to the over-wetted conditions before the rain event.

For medium sand shown in Fig. 7(C–D), the 0.5 % X.G. slopes have reduced erosion during RE 3 but experience much more erosion in RE 5, with the 17° and 21° slopes experiencing 10.2 and 13.6 times more, respectively, than the untreated slopes. The water runoff follows the same trend. After RE 3, there was little erosion in the untreated hydrophobic slopes. The water runoff stayed consistent with an increase, decrease, and another increase from RE to RE. After applying the cured 3 % X.G. treatment, the slopes produced little change in erosion values but at a higher rain intensity than before, yet still more than the untreated slopes. The treated slopes then see a spiked increase in erosion during RE 9, much like the fine sand-treated slopes. This is explained by the pre-formed channels from before the slopes were re-covered, with enhanced erosion occurring along those channels. Recall Fig. 5 and Fig. 6, showing the slopes were not completely dry from RE 8 when RE 9 occurred, leading the already saturated XG-sand mix to slide down in pieces instead of a hardened crust protecting the slope before being over-wetted.

Fig. 7E–F show that the coarse sand 0.5 % X.G. 17°, while initially reducing erosion during RE 3, produced more during RE 5, much like the medium sand treated slopes. Both treated angles yielded less erosion than the untreated slopes during RE 7 and continued that trend after re-covering with cured 3 % X.G. Once again, there was an increase in erosion from RE 9, but not to a large extent as the most significant increase was in the 21° treated slope, from 1.92 to 6.11 mg/cm$^2$. During REs 3, 5, and 9, the water runoff produced from the treated slopes was higher.

Fig. 8 shows the cumulative erosion and water runoff for each angle and treatment type for fine, medium, and coarse sands. The most erosion with the 0.5 % X.G. treatment for fine sand occurred during RE 3 and RE 5 for medium and coarse sand. The data collected from each RE shows that erosion trends are similar when X.G. is used.

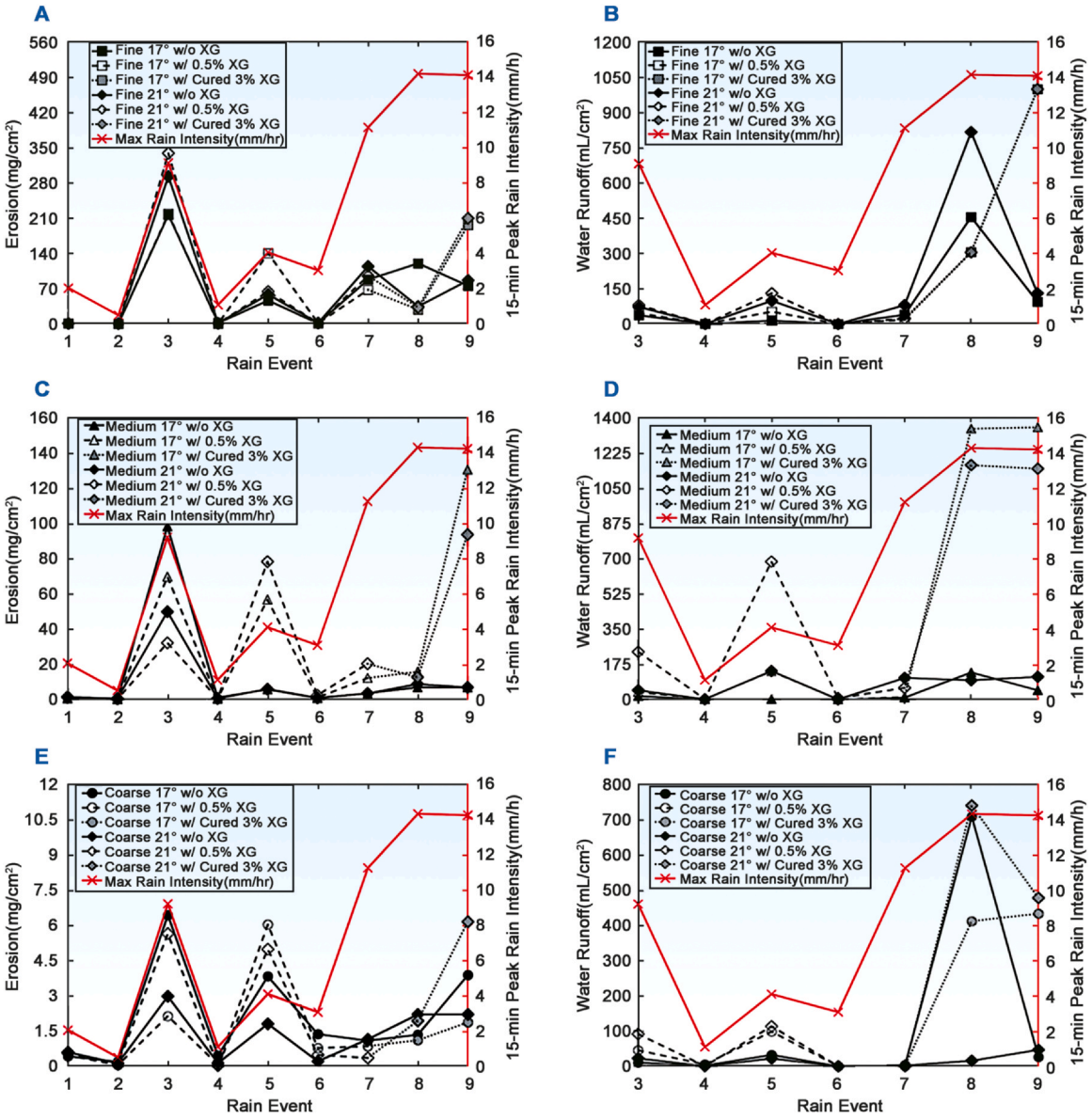



**Fig. 7.** Sand erosion and water runoff data with the 15-min peak rain intensities: (**A–B**) Fine sand; (**C–D**) Medium sand; (**E–F**) Coarse sand.

For all sand types and both angles, the X.G. treated slopes follow the same trends but at different levels, with the fine sand slopes eroding the most with a cumulative erosion of 700.35 mg/cm$^2$ averaged between the angles, coarse sand slopes the least with 16.63 mg/cm$^2$, and medium sand slopes eroding in between the two with 261.50 mg/cm$^2$. However, the untreated hydrophobic slopes do not have similar trends between each sand except for the erosion from RE 3. Untreated fine sand erosion increases from RE to RE with different slopes, while the coarse sand cumulative trend is more linear. It can also be seen that after the initial erosion from RE 3, medium sand erosion is small and linear.

When comparing the cumulative water runoff for each sand, once again, the water runoff follows a similar trend from sand to sand for untreated and 0.5 % X.G. treated slopes, with the 0.5 % X.G. 21° slope producing more overall water runoff during R.E.s 3 and 5 but maintain the same trend. A much higher water runoff occurs when the X.G. is 3 %. It can be noted that the water runoff slopes between R.E.s 8 and 9 go from steeper, linear, and shallower from fine, medium, and coarse sands. This is explained through the saturation of the slopes, where most of the fine sand slope was still over-saturated from the previous RE, and the coarse sand slopes were the least over-saturated, allowing the XG-sand mixture to absorb water, producing less water runoff. For the X.G. treated slopes, those with medium sand accumulated the most water runoff, with 3079.58 mL/cm$^2$ averaged between the angles, fine sand slopes, less than half of the medium slopes, producing 1488.10 mL/cm$^2$, and the least were coarse sand slopes with 1200.11 mL/cm$^2$.

### 3.3. Discussion

Biopolymer applications are financially comparable and potentially more favorable than standard mulching on burned slopes. An alternative surface treatment includes mulching, with an average cost of about $5 per bag covering 0.74 m$^2$ when spread 4 cm deep X.G. price is $7.16 per 500 g in bulk, and if mixed with sand at 3 % for a 4 cm deep layer, it means that 0.0012 m$^3$ or 192 g (X.G. specific gravity is 1.6) costs $2.8 to cover 1 m$^2$, with sand price being $35 per 453.6 kg, which is about $0.5. The cost of X.G. is almost half the price of the mulch material. Installation of mulch costs $85 per 0.77 m$^3$, but the labor cost may vary worldwide, as well as spraying X.G., sand, and water from drones. Application from the air is favorable for steep and unapproachable hillslopes, while mulching is typically performed only along roads.

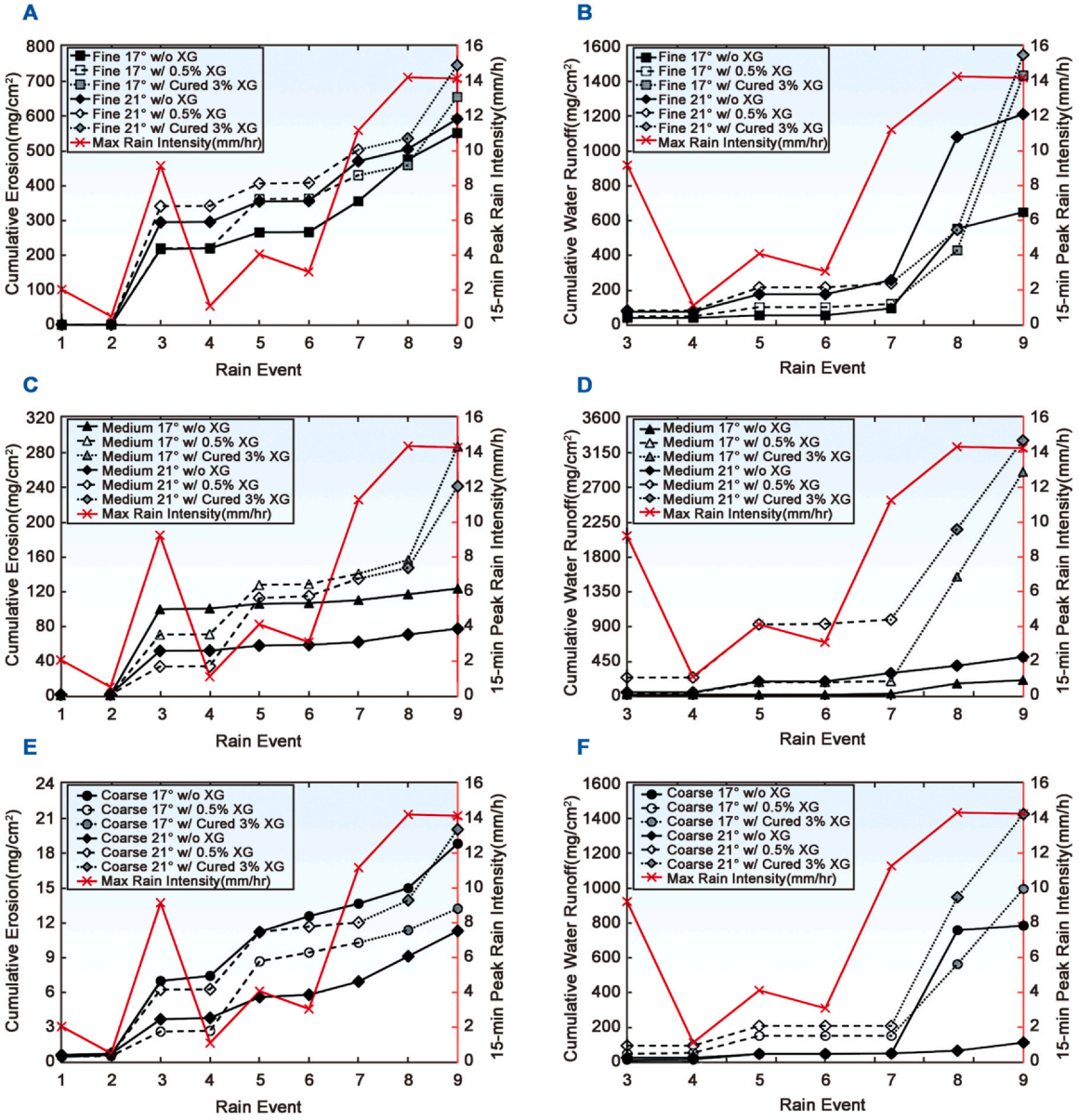



**Fig. 8.** Cumulative erosion and water runoff with the 15-min peak rain intensities: (**A–B**) Fine sand; (**C–D**) Medium sand; (**E–F**) Coarse sand.

## 4. Conclusions

Wildfire-mudflow frequency has increased recently, posing threats to the environment, people, and civil infrastructure. Burned scars are more susceptible to debris flows upon rain on slopes that have lost vegetation and whose surficial soil layers have turned hydrophobic. This paper uses various slopes at high and low rain intensities to explore the advantages and limitations of surficial soil improvement of burned scars with biopolymer, specifically X.G. Furthermore, experimental flumes exposed to environmental conditions provide a unique insight into the resilience and constraints of the proposed treatments.

This study concludes that, despite the limited literature, sprinkling surfaces with X.G. does not yield sufficient stability against erosion for prolonged rains. Furthermore, a different technique is proposed, which pre-mixes X.G. and sand in a dry state and then spreads and wets the mix over hydrophobic slopes. Curing the pluviated sand and X.G. mix for a day after wetting decreases the sand runoff and keeps the water runoff relatively low. However, we classified the surface morphology of treated slopes after the low and high-intensity rain and identify possible pitfalls.

Specifically, fine, medium, and coarse severely hydrophobic sand, 10° to 30° sloped surfaces, covered with a layer of XG-sand mix at 1 %–3 % mass ratios, were tested under 15 mm/h and 50 mm/h rain intensities. Increasing sand coarseness plays a significant positive role in X.G. erosion control. Higher X.G. percentage is needed only for the steepest slopes at the highest rain intensities for coarse sand. In medium and fine sands, erosion control is slightly ceasing; for example, in fine sands, lower 1 % and 2 % X.G. fine sand mixes perform poorly at 25°, at high rain intensities.

Despite surficial improvements, the water runoff can be high without erosion, indicating limited infiltration capabilities. Furthermore, both water and sand runoff increase exponentially once the erosion starts. It is essential to consider the expectancy of rain because this study shows modified surface morphology formed during the rain event. Some experiments show the development of ridges that can further erode during rain. Therefore, this study recommends a practical X.G. percentage of the mix for slope improvement, relying on results at a 25° angle. The surface erosion types were similar for coarse and medium sand, making 2 % X.G. the most material-efficient while having negligible erosion with the same water runoff seen with 3 % X.G.

With natural rain events, tree debris, and animal activity interacting with the hydrophobic slopes, the study offers real-world performance after applying X.G.-sand mixtures as a slope stability mitigation technique. The environmental flume results validate conclusions from rain simulator experiments. Using X.G. as a slope stability technique provides similar erosion and water runoff trends under environmental conditions for all three sand types tested, with fine sand slopes eroding the most.

Insight into the performance of cured 3 % X.G.-sand mixes on slopes with pre-existing channels leads to a conclusion that on burned slopes, in nature, previously formed channels significantly affect performance. It is recommended to use more than 3 % in the X.G.-sand mixture, cautiously considering the frequency of storms in the area and the temperature. Experiments show, for example, a good outcome of 0.5 % X.G. after RE 5 because the slopes were completely dry three days later before RE 6 in early October. However, after 3 % X.G. applied and after RE 8 in mid-December, 12 days was not enough to completely dry the slopes, resulting in significantly increased erosion during RE 9.

## CRediT authorship contribution statement

**Tomac Ingrid:** Writing – review & editing, Resources, Methodology, Funding acquisition, Data curation, Conceptualization. **De Rosas Jonathon Chavez:** Writing – review & editing, Writing – original draft, Methodology, Investigation, Formal analysis, Conceptualization.

## Data availability

Some or all data, models, or codes that support the findings of this study are available from the corresponding author upon reasonable request.

## Declaration of Competing Interest

The authors declare the following financial interests/personal relationships which may be considered as potential competing interests: Ingrid Tomac reports financial support was provided by University of California Institute of Transportation Studies from the State of California. The other authors declare that they have no known competing financial interests or personal relationships that could have appeared to influence the work reported in this paper.

## Acknowledgements

This study was made possible through funding received by the University of California Institute of Transportation Studies from the State of California through the Public Transportation Account and the Road Repair and Accountability Act of 2017 (Senate Bill 1). The contents of this report reflect the views of the author(s), who is/are responsible for the facts and the accuracy of the information presented. This document is disseminated under the sponsorship of the State of California in the interest of information exchange and does not necessarily reflect the official views or policies of the State of California.

## References

Akin, I. D., Garnica, S. S., Robichaud, P. R., & Brown, R. E. (2022). Surficial stabilization of wildfire-burnt hillslopes using xanthan gum and polyacrylamide. *Geotechnical and Geological Engineering, 40*(3), 1187–1200. https://doi.org/10.1007/s10706-021-01951-4

Alexandre, M., & Dubois, P. (2000). Polymer-layered silicate nanocomposites: preparation, properties and uses of a new class of materials. *Materials Science and Engineering: R: Reports, 28*(1), 1–63. https://doi.org/10.1016/S0927-796X(00)00012-7

Ayeldeen, M. K., Negm, A. M., & El Sawwaf, M. A. (2016). Evaluating the physical characteristics of biopolymer/soil mixtures. *Arabian Journal of Geosciences, 9*(5), 371–384. https://doi.org/10.1007/s12517-016-2366-1

Cabalar, A., Wiszniewski, M., & Skutnik, Z. (2017). Effects of xanthan gum biopolymer on the permeability, odometer, unconfined compressive and triaxial shear behavior of a sand. *Soil Mechanics and Foundation Engineering, 54*(5), 356–361. https://doi.org/10.1007/s11204-017-9481-1

Carvalho, S. C. P., de Lima, J. L. M. P., & de Lima, M. I. P. (2014). Using meshes to change the characteristics of simulated rainfall produced by spray nozzles. *International Soil and Water Conservation Research, 2*(2), 67–78. https://doi.org/10.1016/S2095-6339(15)30007-1

Chen, R., Lee, I., & Zhang, L. (2015). Biopolymer stabilization of mine tailings for dust control. *Journal of Geotechnical and Geoenvironmental Engineering, 141*(2), Article 04014100. https://doi.org/10.1061/(ASCE)GT.1943-5606.0001240

Akin, I.D. and Likos, W.J. (2016). Water vapor sorption of polymer-modified bentonites. Geo-Chicago 2016, ASCE, Reston, VA, 508–517. https://doi.org/10.1061/9780784480144.050.

CNRFC and NOAA (2021). CNRFC Data Archive, ⟨https://www.cnrfc.noaa.gov/arc_search.php⟩.

Crockford, H., Topalidis, S., & Richardson, D. P. (1991). Water repellency in a dry sclerophyll eucalypt forest — measurements and processes. *Hydrological Processes, 5*(4), 405–420. https://doi.org/10.1002/hyp.3360050408

DeBano, L. F. (1967). *Soil Wettability and Wetting Agents: Out Current Knowledge of the Problem, 43*. Pacific Southwest Forest and Range Experiment Station, Forest Service, U.S. Department of Agriculture.

DeBano, L. F. (1981). *Water repellent soils: a state-of-the-art, 46*. U.S. Department of Agriculture, Forest Service, Pacific Southwest Forest and Range Experiment Station.

DeBano, L. F., & Krammes, J. S. (1966). Water repellent soils and their relation to wildfire temperatures. *Hydrological Sciences Journal, 11*(2), 14–19. https://doi.org/10.1080/02626666609493457

Doerr, S. H., Shakesby, R. A., & Walsh, R. P. D. (1996). Soil hydrophobicity variations with depth and particle size fraction in burned and unburned Eucalyptus globulus and Pinus pinaster forest terrain in the Agueda Basin, Portugal. *Catena, 27*(1), 25–47. https://doi.org/10.1016/0341-8162(96)00007-0

Doerr, S. H., Shakesby, R. A., & Walsh, R. P. D. (2000). Soil water repellency: Its causes, characteristics and hydro-geomorphological significance. *Earth-Science Reviews, 51*(1–4), 33–65. https://doi.org/10.1016/S0012-8252(00)00011-8

Gioia, F., & Ciriello, P. P. (2006). The containment of oil spills in porous media using xanthan/aluminum solutions, gelled by gaseous $CO_2$ or by $AlCl_3$ solutions. *Journal of Hazardous Materials, 138*(3), 500–506. https://doi.org/10.1016/j.jhazmat.2006.05.095

Ham, S.-M., Chang, I., Noh, D.-H., Kwon, T.-H., & Muhunthan, B. (2018). Improvement of surface erosion resistance of sand by microbial biopolymer formation. *Journal of Geotechnical & Geoenvironmental Engineering, 144*(7), Article 06018004. https://doi.org/10.1061/(ASCE)GT.1943-5606.0001900

Helvey, J. D. (1980). Effects of a north central Washington wildfire on runoff and sediment production. *JAWRA Journal of American Water Resources Association, 16*(4), 627–634. https://doi.org/10.1111/j.1752-1688.1980.tb02441.x

Huffman, E. L., MacDonald, L. H., & Stednick, J. D. (2001). Strength and persistence of fire-induced soil hydrophobicity under ponderosa and lodgepole pine, Colorado Front Range. *Hydrological Processes, 15*(15), 2877–2892. https://doi.org/10.1002/hyp.379

Joga, J. R., & Varaprasad, B. J. S. (2020). Effect of xanthan gum biopolymer on dispersive properties of soils. *World Journal of Engineering, 17*(4), 563–571. https://doi.org/10.1108/WJE-05-2020-0152

Khachatoorian, R., Petrisor, I. G., Kwan, C.-C., & Yen, T. F. (2003). Biopolymer plugging effect: laboratory-pressurized pumping flow studies. *Journal of Petroleum Science and Engineering, 38*(1–2), 13–21. https://doi.org/10.1016/S0920-4105(03)00019-6

Lee, S., Im, J., Cho, G.-C., & Chang, I. (2019). Laboratory triaxial test behavior of xanthan gum biopolymer-treated sands. *Geomechanics and Engineering, 17*(5), 445–452. https://doi.org/10.12989/gae.2019.17.5.445

Department of Forestry and Fire Protection (2022). "Stats & events." *Cal Fire*, ⟨https://www.fire.ca.gov/stats-events/⟩.

Kavazanjian Jr., E., Iglesias, E., and Karatas, I. (2009). "Biopolymer soil stabilization for wind erosion control." Proceedings of the 17th International Conference on Soil Mechanics and Geotechnical Engineering (Volumes 1, 2, 3 and 4), IOS press, 881–884. https://doi.org/10.3233/978-1-60750-031-5-881.

Law S.L.G., Kuok K.K. and Trinidad S.G. (2021). "Rainfall Intensities and Raindrop Size Distribution Characteristics". The 13th International UNIMAS Engineering Conference 2020 (ENCON 2020), IOP Conf. Ser.: Mater. Sci. Eng. 1101 012009.

Martner, B. E., Yuter, S. E., White, A. B., Matrosov, S. Y., Kingsmill, D. E., & Ralph, F. M. (2008). Raindrop size distributions and rain characteristics in California coastal rainfall for periods with and without a radar bright band. *Journal of Hydrometeorology, 9*, 408–425. https://doi.org/10.1175/2007JHM924.1

Meeuwig, R.O. (1971). Infiltration and water repellency in granitic soils, Vol. 111. Intermountain Forest & Range Experiment Station, Forest Service, U.S. Department of Agriculture.

Moghal, A. A. B., & Vydehi, K. V. (2021). State-of-the-art review on efficacy of xanthan gum and guar gum inclusion on the engineering behavior of soils. *Innovative Infrastructure Solutions, 6*(2), 1–14. https://doi.org/10.1007/s41062-021-00462-8

Movasat, M., & Tomac, I. (2020a). Evaluation and remediation of post-wildfire slope stability (EDP Sciences) *E3S Web of Conferences, 205*, 04007. https://doi.org/10.1051/e3sconf/202020504007

Movasat, M., & Tomac, I. (2020). Post-fire mudflow prevention by biopolymer treatment of water repellent slopes. In *Geo-Congress 2020* (pp. 170-178). Reston, VA: American Society of Civil Engineers. https://doi.org/10.1061/9780784482834.019

Movasat, M., & Tomac, I. (2020c). Assessment of physical properties of water-repellent soils. *Journal of Geotechnical and Geoenvironmental Engineering, 147*(9), Article 06021010.

Movasat, M., & Tomac, I. (2022a). *The effect of grain size on rainfall-triggered debris flow in hydrophobic granular slopes. Geo-Congress 2022, March 20–23, 2022, Charlotte, North Carolina, 335*, ASCE417–424.

Movasat, M., & Tomac, I. (2022b). *Evaluation of Post-Impact Behavior of Single Droplet on the Hydrophobic Soil Surface. Geo-Congress 2022, March 20–23, 2022, Charlotte, North Carolina, 335*, ASCE425–432.

Movasat, M., De La Cruz, A., & Tomac, I. (2023). Role of hydrophobic sand particle granularity on water droplet post-impact dynamics. *International Journal of Multiphase Flow, 167*, Article 104529. https://doi.org/10.1016/j.ijmultiphaseflow.2023.104529

Movasat, M., & Tomac, I. (2025). Kinematics of post-wildfire debris flow initiation mechanism: impact of hydrophobic layer spatial variability and particle size. *Canadian Geotechnical Journal, 62*, 1–18. https://doi.org/10.1139/cgj-2023-053

Nanko, K., Hotta, N., & Suzuki, M. (2006). Evaluating the influence of canopy species and meteorological factors on throughfall drop size distribution. *Journal of Hydrology, 329*, 422–431. https://doi.org/10.1016/j.jhydrol.2006.02.036

Oakley, N. S., Lancaster, J. T., Kaplan, M. L., et al. (2017). Synoptic conditions associated with cool season post-fire debris flows in the Transverse Ranges of southern California. *Natural Hazards, 88*(1), 327–354. https://doi.org/10.1007/s11069-017-2867-6

Oakley, N. S., & Redmond, K. T. (2014). A climatology of 500-hPa closed lows in the northeastern pacific ocean, 1948–2011. *Journal of Applied Meteorology and Climatology, 53*(6), 1578–1592. https://doi.org/10.1175/JAMC-D-13-0223.1

Ralph, F. M., Prather, K. A., Cayan, D., Spackman, J. R., DeMott, P., Dettinger, M., ... Intrieri, J. (2016). CalWater field studies designed to quantify the roles of atmospheric rivers and aerosols in modulating U.S. west coast precipitation in a changing climate. *Bulletin of the American Meteorological Society, 97*(7), 1209–1228. https://doi.org/10.1175/BAMS-D-14-00043.1

Saulick, Y., Lourenco, S. N. D., & Baudet, B. A. (2017). A semi-automated technique for repeatable and reproducible contact angle measurements in granular materials using the sessile drop method. *Soil physics and hydrology, 81*(2), 241–249. https://doi.org/10.2136/sssaj2016.04.0131

Savage, S. M. (1974). Mechanism of fire-induced water repellency in soil. *Soil Science Society of America Journal, 38*(4), 652–657. https://doi.org/10.2136/sssaj1974.03615995003800040033x

Scott, D. F., & Van Wyk, D. B. (1990). The effects of wildfire on soil wettability and hydrological behavior of an afforested catchment. *Journal of Hydrology, 121*(1–4), 239–256. https://doi.org/10.1016/0022-1694(90)90234-O

Soldo, A., Miletić, M., & Auad, M. L. (2020). Biopolymers as a sustainable solution for the enhancement of soil mechanical properties. *Scientific Reports, 10*(1), 1–13. https://doi.org/10.1038/s41598-019-57135-x

NOAA (2011). National Weather Service Glossary: Closed Low, ⟨https://forecast.weather.gov/glossary.php?word=closed+low⟩.

Tiwari, B., Ajmera, B., Gonzalez, A., Sonbol, H. (2020). "Impact of Wildfire on Triggering Mudslides—A Case Study of 2018 Montecito Debris Flows." Geo-Congress 2020: Engineering, Monitoring, and Management of Geotechnical Infrastructure, ASCE, Reston, VA, 40–49. https://doi.org/10.1061/9780784482797.005.

Tran, A. T. P., Chang, I., & Cho, G.-C. (2019). Soil water retention and vegetation survivability improvement using microbial biopolymers in drylands. *Geomechanics and Engineering, 17*(5), 475–483. https://doi.org/10.12989/gae.2019.17.5.475